OPEN ACCESS Freely available online
CC BY

T. Risse, S. Bilbao, and T. Helie,
"Robust and Real-Time Physical Modeling
Sound Synthesis for Nonlinear Systems: String Vibration,"
J. Audio Eng. Soc., vol. 74, no. 7/8, pp. 485–496 (2026 Jul./Aug.).
https://doi.org/10.17743/jaes.2026.0271.

Robust and Real-Time Physical Modeling Sound Synthesis for Nonlinear Systems: String Vibration

THOMAS RISSE,* **STEFAN BILBAO,** *AES Member* **AND THOMAS HELIE**
(thomas.risse@ircam.fr) (stefan.bilbao@ircam.fr) (thomas.helie@ircam.fr)

STMS Laboratory, IRCAM-CNRS-Sorbonne University, Paris, France

The aim of physical modeling is to allow for realistic rendering of musical sound based purely on a mathematical description of a dynamical system. For expressive musical use, real-time performance is essential. But other major concerns are the requirement for numerical stability, perceptual fidelity, and robustness. Fulfilling these simultaneous requirements for strongly nonlinear systems is challenging. In the case of nonlinear string vibration, stability may be ensured by enforcing a numerical energy balance, and recently, efficient explicit methods have become available based on the use of scalar auxiliary variable techniques. However, convergence rates can be slow and seem to be system-dependent. Especially for musical use, numerical drift of the auxiliary variable over long time scales can result in dramatic unwanted effects, including pitch drifts after several impacts on the same resonator. In this paper, a novel method for mitigating this unwanted drift while preserving power balance is presented. A set of modified equations is proposed to control the drift artifact through an energy-balanced feedback-loop. Numerical experiments are run to check convergence on simulations with three different nonlinearities. A real-time implementation is provided as a Max/MSP external, enabling up to 60-note polyphony on a laptop.

Keywords: numerical methods, port-Hamiltonian systems, scalar auxiliary variable

1 INTRODUCTION

Physical modeling synthesis [1–3] as an exercise in numerical simulation is computationally demanding, and yet relatively complex musical systems are coming within reach of the real-time threshold that is essential for musical use. Systems exhibiting strong distributed nonlinearities, such as the string vibrating at high amplitudes, require careful numerical design to run efficiently. Three core requirements are

- (A) Efficient operation,
- (B) Numerical stability, and
- (C) Robustness of the computed solutions.

For strongly nonlinear systems, numerical methods based on the principle of an energy balance are probably the only means of addressing the stability requirement (B) above. These can be viewed as extensions of geometric (structure-preserving) numerical integration methods [4]; many existing schemes, such as the discrete gradient methods [5] or projection methods [6, SEC. 5.3.3] rely on solving implicit nonlinear equations for which iterative solvers such as Newton-Raphson are required. These are computationally prohibitive for real-time musical use, conflicting with the efficiency requirement (A) and not always convergent and stable for a fixed number of iterations per step, conflicting with both requirements (B) and (C).

For systems of cubic nonlinear type, including some models of string vibration and plate vibration at high amplitudes, it is possible to arrive at schemes satisfying an energy balance, and with provable numerical stability conditions, see [3, chapter 8]. Such schemes are in general *linearly implicit* and require the construction and solution of a linear system at each time step. Unconditionally stable *linearly implicit* methods [7] have also been proposed in the context of nonlinear port-Hamiltonian systems [8, 9]. This avoids the use of nonlinear iterative solvers but is still too computationally costly for real-time use.

The recently introduced invariant energy quadratization method [10] is based on the simulation of the state space augmented by a distributed variable storing the square root of the energy density. Slightly later, the scalar auxiliary vari-

*To whom correspondence should be addressed, email: thomas.risse@ircam.fr

able (SAV) method [11] was introduced, for which the state space is augmented by a lumped variable storing the square root of the total potential energy of the system. The strength of these methods lies in the fact that the energy of the system may be expressed as a quadratic functional of the state variables, making any quadratic invariant preserving scheme a good candidate for stable simulations [12]. See [13] for an example of an SAV method applied in the present case of nonlinear string vibration. Such methods remain, however, linearly implicit, and still do not address (A) above. More recently, *fully explicit* SAV methods satisfying an energy balance for a general class of Hamiltonian systems [14] have been developed. In this case, matrix structure is exploited to avoid the linear system solution entirely (through the use of the Sherman-Morrison identity[15]). See [16–18] for musical applications, including in real time [19]. Thus, (A) and (B) are effectively solved.

Problem (C) remains however. SAV methods rely on reformulating the Hamiltonian (energy) of the system as a quadratic function of an *extended* state space. Although this allows the construction of fully explicit energy-preserving schemes, it also generates a drawback. Indeed, the extended state space can be viewed as an overparametrization of the system, with a hidden constraint between the auxiliary variable and the original state variables. This hidden constraint is in general not satisfied by the explicit schemes available because of what is called here "the auxiliary variable drift," leading to audibly bad long-term behavior of the simulations. Reference [20] discusses this issue and convergence properties of different schemes for the musical string, clearly indicating that this problem is not trivial. For distributed noncontact nonlinearities, in [17] it is mentioned that the original SAV algorithm works well in the case of the Kirchhoff-Carrier model (KC) but exhibits auxiliary variable drift for a more complex nonlinearity (fourth-order Taylor expansion of the geometrically exact string model to transverse vibrations only, named GE4 in the current paper).

To solve this issue, Russo et al. [21] propose the imposition of a positive sign constraint on the auxiliary variable (inspired by previous work on collision problems, see [22]). This sign-constraint-based method does not introduce numerical dissipation and works well when the auxiliary variable drifts to negative values. However, depending on the system, the auxiliary variable may also drift upward (having higher values than what it should). In this case, sign-constraint-based methods are ineffective. Comparisons between the proposed method and sign-constraint-based methods are given in SEC. 6.3. Outside the musical acoustics community, the drift problem is also well known: reference [23] introduces a relaxation step correcting the value of the auxiliary variable to minimize the drift by solving an optimization problem, for which an efficient solution is derived in [24]. These relaxation-step approaches solve the drift issue while ensuring stability but rely on the original system being dissipative, which is a problem when simulating nearly lossless musical instruments.

In this paper, the authors present a novel method to address the auxiliary variable drift problem and cope with problem (C) above. The approach is based on a modification of the continuous time equations by introducing an energy-balanced feedback loop designed to stabilize the drift of the auxiliary variable, even when subjected to perturbations. This method is suitable for port-Hamiltonian systems with quadratic kinetic energy and smooth nonquadratic potential energy. It is applied to a variety of nonlinear string models, a relevant case for musical acoustics. The scheme is also implemented in a Max/MSP[1] external, which is publicly available, along with example sounds and an interactive browser-based simulation on the companion web page (https://ircam-rnd.github.io/SAV-string-simulations/).

The paper is organized as follows: SEC. 2 presents the string model and its spatial discretization approximation using finite differences. SEC. 3 reviews the SAV transformation. As a main contribution, SEC. 4 proposes a modification of the dynamical system in the continuous time domain, based on a power-balanced control approach, to reduce any SAV drift (e.g., resulting from inconsistent initial conditions or numerical errors). An interleaved time-stepping scheme is provided in SEC. 5 and evaluated through numerical experiments in SEC. 6. SEC. 7 discusses the real-time implementation and is followed by a general conclusion in SEC. 8. This paper is expanded from [25], presented at the 28th International Conference on Digital Audio Effects in Ancona, Italy.

2 ENERGY CONSISTENT MODELING

2.1 Nonlinear String Equations, Continuous Space

Consider the nonlinear dynamics of a stiff string. The transverse displacement $u(x, t)$ is governed by the following second-order partial differential equation (PDE; see [26] for geometrically exact string equations and [27] for their reduction to transverse vibrations only resulting in the following formulation):

$$\begin{aligned}\rho A\,\partial_t^2 u &= (T\partial_x^2 - EI\partial_x^4)u - 2\rho A(\eta_0 - \eta_1\partial_x^2)\partial_t u \\ &+\partial_x\left(\phi'(\partial_x u)\right) + \delta_{x_{\text{in}}} f_{\text{in}}\end{aligned} \tag{1}$$

for $(x, t) \in \Omega \times (0, +\infty)$ with $\Omega = (0, l_0)$ for some string length l_0 in m. The various parameters, all assumed constant, are the radius R in m, cross-section $A = \pi R^2$ in m^2, moment of inertia $I = \pi R^4/4$ in m^4, density ρ in kg m^{-3}, string tension T in N, Young's modulus E in pascals (Pa), and dissipation coefficients η_0 and η_1. The total force $f_{\text{in}}(t)$ in newtons (N) is the driving term applied through the spatial Dirac distribution $\delta_{x_{\text{in}}}(x) = \delta(x - x_{\text{in}})$ at x_{in} (in m^{-1}). ∂_t and ∂_x represent partial differentiation with respect to t and x, respectively.

Boundary conditions are fixed as $u = 0$ and $\partial_x^2 u = 0$ at extremities $x \in \partial\Omega = \{0, l_0\}$ (simply-supported). Initial conditions on u and $\partial_t u$ at $t = 0$ are zero or specified later.

$\phi(\partial_x u)$ represents a nonlinear contribution to the potential energy of the string. This density can take various forms. In this work, three versions of decreasing complexity are

[1] https://github.com/Ircam-RnD/SAV-string-simulations.

Table 1. Potentials and associated nonlinear force densities.

Name	$\phi(\zeta := \partial_x u)$	$F_{nl}(\zeta := \partial_x u)$
GE	$\frac{EA-T}{2}\left(\sqrt{1+\zeta^2}-1\right)^2$	$(EA-T)\partial_x\left(\zeta\frac{\sqrt{1+\zeta^2}-1}{\sqrt{1+\zeta^2}}\right)$
GE4	$\frac{EA-T}{8}\zeta^4$	$\frac{EA-T}{2}\partial_x(\zeta^3)$
KC	$\frac{EA}{8l_0}\|\|\zeta\|\|^2_{\mathrm{L}^2(\Omega)}\zeta^2$	$\frac{EA}{2l_0}\|\|\zeta\|\|^2_{\mathrm{L}^2(\Omega)}\partial_x\zeta$

considered: the reduction of the the geometrically exact string model of [26] to transverse vibrations only (named GE), a fourth-order Taylor expansion of this model (GE4), and KC, which effectively averages the nonlinearity along the string. The force density $F_{nl}(\partial_x u) = \partial_x(\phi'(\partial_x u))$ depends on the derivative ϕ' of the potential ϕ chosen in Table 1.

2.2 A General Model Structure

Although the method developed in this paper is demonstrated for the specific case of nonlinear string vibration, it is developed in a general manner for a larger class of systems. Consider a system described by its state $\boldsymbol{\alpha} = [\mathbf{p}, \mathbf{q}]^\intercal$ including vectors of generalized coordinates $\mathbf{q}$ and momenta $\mathbf{p}$. Under quite broad assumptions, a Hamiltonian or total energy may be defined as

$$H(\mathbf{p},\mathbf{q}) = \frac{1}{2}\mathbf{p}^\intercal\mathbf{M}^{-1}\mathbf{p} + \underbrace{\frac{1}{2}\mathbf{q}^\intercal\mathbf{K}\mathbf{q} + E_{\mathrm{nl}}(\mathbf{q})}_{V(\mathbf{q})}, \tag{2}$$

with mass matrix $\mathbf{M}$ and stiffness matrix $\mathbf{K}$ both assumed symmetric and positive definite. The potential energy $V(\mathbf{q})$ is the sum of a quadratic term and a general positive function of the generalized coordinates $E_{\mathrm{nl}}(\mathbf{q})$, with $E_{\mathrm{nl}}(\mathbf{0}) = 0$. Hamilton's equations may be written as

$$\frac{\mathrm{d}}{\mathrm{dt}}\mathbf{p} = -\nabla_{\mathbf{q}}H, \quad \frac{\mathrm{d}}{\mathrm{dt}}\mathbf{q} = \nabla_{\mathbf{p}}H \tag{3}$$

and describe the dynamics of the system in the lossless and unforced case.

To account for losses and external forcing, a positive semidefinite dissipation matrix $\mathbf{R}_0$ and an input (control) vector $\mathbf{u}$ are defined. The dynamics are augmented as

$$\underbrace{\begin{bmatrix}\frac{\mathrm{d}}{\mathrm{dt}}\mathbf{p}\\ \frac{\mathrm{d}}{\mathrm{dt}}\mathbf{q}\end{bmatrix}}_{\dot{\boldsymbol{\alpha}}} = \left(\underbrace{\begin{bmatrix}0 & -\mathbb{I}\\ \mathbb{I} & 0\end{bmatrix}}_{\mathbf{J}} - \underbrace{\begin{bmatrix}\mathbf{R}_0 & 0\\ 0 & 0\end{bmatrix}}_{\mathbf{R}}\right)\underbrace{\begin{bmatrix}\mathbf{M}^{-1}\mathbf{p}\\ \mathbf{K}\mathbf{q}+\nabla E_{\mathrm{nl}}(\mathbf{q})\end{bmatrix}}_{\nabla H} + \begin{bmatrix}\mathbf{G}_p\\ 0\end{bmatrix}\mathbf{u}. \tag{4}$$

The system in Eq. (4) satisfies the continuous-time power balance:

$$\begin{aligned}\frac{\mathrm{d}}{\mathrm{dt}}H(\mathbf{p},\mathbf{q}) &= \nabla H^\intercal\frac{\mathrm{d}}{\mathrm{dt}}\boldsymbol{\alpha},\\ &\overset{(4)}{=} \nabla H^\intercal\left((\mathbf{J}-\mathbf{R})\nabla H + \begin{bmatrix}\mathbf{G}_p\\ 0\end{bmatrix}\mathbf{u},\right)\\ &= -\underbrace{\mathbf{p}^\intercal\mathbf{M}^{-1}\mathbf{R}_0\mathbf{M}^{-1}\mathbf{p}}_{\text{dissipated power}\geq 0} + \underbrace{\mathbf{p}^\intercal\mathbf{M}^{-1}\mathbf{G}_p\mathbf{u}}_{\text{external power}},\end{aligned} \tag{5}$$

accounting for variations of energy resulting from dissipated power and external forcing.[2] The above formulation is a discrete port-Hamiltonian system (see e.g., [9]), effectively a structured state-space model, which allows a power-balance equation [Eq. (5)] to be expressed in a general way. The method presented in this paper is centered around the preservation of this power balance, both in continuous time and discrete time. Note also that Eq. (4) may be recast in an equivalent second-order form as

$$\mathbf{M}\frac{\mathrm{d}^2}{\mathrm{dt}^2}\mathbf{q} = -(\mathbf{K}\mathbf{q} + \nabla E_{\mathrm{nl}}(\mathbf{q})) - \mathbf{R}_0\frac{\mathrm{d}}{\mathrm{dt}}\mathbf{q} + \mathbf{G}_p\mathbf{u}. \tag{6}$$

2.3 Nonlinear String Equations, Discrete Space

To recast the chosen string model in the form of Eq. (4), the equations must be discretized in space. A finite difference method preserving energetic identities is used. It has been used in multiple numerical studies of nonlinear string vibrations (see for example [21]) and will not be detailed here for brevity. The method is also described in a generic way in [28] in the context of port-Hamiltonian systems. It results in a system of the form of Eq. (4) with macroscopic momenta $\mathbf{p} \equiv [p_1, ..., p_{N-1}]^{\mathrm{T}}$ in kg m s^{-1} and transverse displacements $\mathbf{q} \equiv [q_1, ..., q_{N-1}]^{\mathrm{T}}$ in m at the nodes of a spatial grid, with grid spacing h such that $l_0 = Nh$ for integer N. System matrices are

$$\mathbf{M} = h\rho A\mathbb{I}, \quad \mathbf{K} = h(-T\mathbb{I} + EI\,\mathbf{D}^2)\mathbf{D}^2, \tag{7}$$

$$\mathbf{R_0} = -2h\rho A\eta_1\mathbf{D}^2 + 2h\rho A\eta_0\mathbb{I}, \tag{8}$$

$$\mathbf{u} = f_{\mathrm{in}}, \tag{9}$$

with second-order spatial finite difference matrix[2]

$$\mathbf{D}^2 = \frac{1}{h^2}\begin{bmatrix}-2 & 1 & & 0\\ 1 & \ddots & \ddots & \\ & \ddots & \ddots & 1\\ 0 & & 1 & -2\end{bmatrix}. \tag{10}$$

The expression for $E_{\mathrm{nl}}(\mathbf{q})$ is obtained from a finite difference discretization of the integral of the choice of nonlinear potential (see Table 1) over the domain. $\mathbf{f}_{\mathrm{nl}}(\mathbf{q})$ is directly obtained as the gradient of $E_{\mathbf{nl}}(\mathbf{q})$.

Because the spatial discretization procedure is not fully described here, transition from the continuous-space second-order string PDE [Eq. (1)] to the discrete-space first-order ODE described by Eq. (4) with matrices from Eqs. (7–10) may seem unclear. An easier comparison can be made between Eq. (1) and the discrete-space second-order form in Eq. (6) with matrices from Eqs. (7–10). In the following, however, the first-order formulation is used to make apparent symmetries in the SAV variable transformation, which are responsible for the power balance.

[2] Note that $\mathbf{D}^2$ may be viewed as the composition of two first-order finite difference matrices defined on interleaved spatial grids, as presented in [25] and detailed in [28].

3 SCALAR AUXILIARY VARIABLE TRANSFORMATION

SAV methods are used to design efficient energy-stable numerical schemes. There is a large variety of possible state transformations, presented in [29], that may be applied to port-Hamiltonian systems. This work is focused on the original SAV method from [11] that has been used for the simulation of systems like Eq. (4) in the context of musical acoustics in recent years.

The SAV is introduced as

$$r(t) = \sqrt{2E_{nl}(\mathbf{q}) + C_0} \tag{11}$$

and is appended to the system state to yield $\boldsymbol{\alpha}_{\text{sav}} = [\mathbf{p}, \mathbf{q}, r]^\intercal$. $C_0 > 0$ is a gauge constant set to a numerical epsilon to avoid division by zero (see e.g., reference [22]). The Hamiltonian for the extended state space writes as a quadratic function

$$H_{\text{sav}}(\boldsymbol{\alpha}_{\text{sav}}) = \frac{1}{2}\left(\mathbf{p}^\intercal\mathbf{M}^{-1}\mathbf{p} + \mathbf{q}^\intercal\mathbf{K}\mathbf{q} + r^2\right). \tag{12}$$

The dynamics of system Eq. (4) may be rewritten equivalently, using the chain rule, as

$$\begin{bmatrix} \frac{\mathrm{d}}{\mathrm{d}t}\mathbf{p} \\ \frac{\mathrm{d}}{\mathrm{d}t}\mathbf{q} \\ \frac{\mathrm{d}}{\mathrm{d}t}r \end{bmatrix} = \left(\hat{\mathbf{J}} + \mathbf{J}_{\text{sav}}(\boldsymbol{\alpha}_{\text{sav}}) - \hat{\mathbf{R}}\right) \underbrace{\begin{bmatrix} \mathbf{M}^{-1}\mathbf{p} \\ \mathbf{K}\mathbf{q} \\ r \end{bmatrix}}_{\nabla H_{\text{sav}}} + \begin{bmatrix} \mathbf{G}_p \\ 0 \\ 0 \end{bmatrix} u, \tag{13}$$

with extended matrices

$$\hat{\mathbf{J}} = \begin{bmatrix} \mathbf{J} & \mathbf{0} \\ \mathbf{0} & 0 \end{bmatrix}, \hat{\mathbf{R}} = \begin{bmatrix} \mathbf{R} & \mathbf{0} \\ \mathbf{0} & 0 \end{bmatrix} \tag{14}$$

and where the skew-symmetric matrix $\mathbf{J}_{\text{sav}}$ is of the form

$$\mathbf{J}_{\text{sav}}(\boldsymbol{\alpha}_{\text{sav}}) = \begin{bmatrix} \mathbf{0} & \mathbf{0} & -\mathbf{g}(\boldsymbol{\alpha}_{\text{sav}}) \\ \mathbf{0} & \mathbf{0} & \mathbf{0} \\ \mathbf{g}^\intercal(\boldsymbol{\alpha}_{\text{sav}}) & \mathbf{0} & 0 \end{bmatrix}, \tag{15}$$

with $\mathbf{g}(\boldsymbol{\alpha}_{\text{sav}}) := \mathbf{g}_{std}(\mathbf{q}) = \frac{\mathbf{f}_{nl}(\mathbf{q})}{\sqrt{2E_{\text{nl}}(\mathbf{q})+C_0}}$.

Systems in Eqs. (4) and (13–15) are equivalent in the sense that for consistent initial conditions satisfying $r(t_0) = \sqrt{2E_{nl}(\mathbf{q}(t_0)) + C_0}$, they yield the same trajectories in the original state space $[\mathbf{p}, \mathbf{q}]$. Moreover, any trajectory of Eqs. (13–15) generated from consistent initial conditions satisfies relations in Eq. (11) for all $t \geq t_0$.

At first glance, Eqs. (13–15) may seem more complex than Eq. (6), with added redundancy through the introduction of the auxiliary variable r. However, this formulation proves useful to build efficient power-preserving numerical schemes. The power balance equation for the modified system is

$$\begin{aligned} \frac{\mathrm{d}}{\mathrm{d}t}H_{\text{sav}} &= \nabla H_{\text{sav}}^\intercal \frac{\mathrm{d}}{\mathrm{d}t}\boldsymbol{\alpha}_{\mathbf{sav}}, \\ &= \nabla H_{\text{sav}}^\intercal \left(\left(\hat{\mathbf{J}} + \mathbf{J}_{\text{sav}}(\alpha_{\text{sav}}) - \hat{\mathbf{R}}\right)\nabla H_{\text{sav}} + \begin{bmatrix} \mathbf{G}_p \\ 0 \end{bmatrix}\mathbf{u}\right), \\ &= \underbrace{-\mathbf{p}^\intercal\mathbf{M}^{-1}\mathbf{R}_0\mathbf{M}^{-1}\mathbf{p}}_{\text{dissipated power}\geq 0} + \underbrace{\mathbf{p}^\intercal\mathbf{M}^{-1}\mathbf{G}_p\mathbf{u}}_{\text{external power}}, \end{aligned} \tag{16}$$

which is the exact equivalent of Eq. (5). But, as a key point, in the second line of Eq. (16), ∇H_{sav} is a linear function of the state, and the nonlinearity resides in the $\mathbf{J}_{\text{sav}}(\alpha_{\text{sav}})$ matrix. In the design of explicit time-stepping schemes preserving a discrete equivalent to Eq. (16), the main feature is that $\mathbf{J}_{\text{sav}}(\alpha_{\text{sav}})$ can be evaluated explicitly without disturbing the power balance equation as long it remains skew-symmetric.[3]

4 DRIFT CONTROL

The system in Eqs. (13–15) is the key to efficient energy-stable simulation because the corresponding Hamiltonian is quadratic, as discussed in previous work [14] and mentioned at the end of the previous section. However, explicit evaluation of the matrix $\mathbf{J}_{\text{sav}}(\boldsymbol{\alpha}_{\text{sav}})$ may generate drift between numerical values of r and $\sqrt{2E_{nl}(\mathbf{q}) + C_0}$ owing to truncation errors, even for consistent initial conditions. Fig. 1 presents a schematic interpretation of the auxiliary variable drift occurring in energy-preserving cases after time discretization. This drift can have a dramatic effect on simulations, as shown in the numerical experiments in SEC. 6, because the simulated SAV system is then no longer equivalent to the original system. This has been documented in the literature in (e.g., [17, 24, 22]). For some string models, the auxiliary variable drift can cause a progressive degradation of the numerical results for successive strikes of the string, as can be seen in Fig. 4.

The main contribution of this paper is the introduction of a new method reducing the impact of the numerical drift problem and thus allowing reliable musical use. The proposed approach used here is to add a control term to the system in Eqs. (13–15) *before* time discretization, guided by a set of requirements.

- (R0): The (scalar) drift measure

  $$\epsilon = f_\epsilon(\mathbf{q}, r) = r - \sqrt{2E_{nl}(\mathbf{q}) + C_0}, \tag{17}$$

  is governed by the control law

  $$\frac{d}{dt}\epsilon = -\frac{1}{\tau_0}\epsilon, \tag{18}$$

  where τ_0 is a characteristic control time.
- (R1): The drift controller must not change the global power balance. Consequently, it must be expressible as a skew-symmetric modification of the interconnection matrix $\mathbf{J}_{\text{sav}}$ in Eq. (13).
- (R2): The dynamics of the modified system must reduce to that of the system in Eqs. (13–15) if $\epsilon = 0$.

[3] The last line of the power computation relies on the skew-symmetry of $\mathbf{J}$. Indeed, for a skew-symmetric matrix $\mathbf{J}$, $\mathbf{x}^\intercal\mathbf{J}\mathbf{x} = 0$. Note also that the external power can be written as $\mathbf{y}^\intercal u$, where $y = \mathbf{G}_p^\intercal\mathbf{M}^{-1}\mathbf{p}$ is identified as the power-conjugated output of the system.

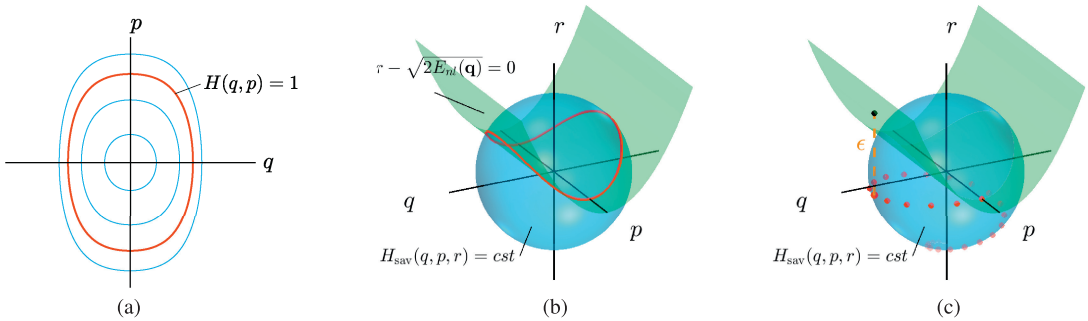


Fig. 1. Representation of state-space trajectories at different steps of the discretization procedure, illustrating the drift issue. For visualization purposes, the system is supposed to have a single degree of freedom. It can be viewed as a Duffing oscillator. The blue lines and surfaces correspond to isovalues of the Hamiltonian. The green surfaces correspond to the SAV in Eq. (11) in the augmented state space. The red lines correspond to continuous time solutions, and the red dots correspond to a hypothetical numerical solution exhibiting auxiliary variable drift. The drift problem is summarized as follows: available explicit numerical schemes generate solutions on the blue ball, hence ensuring stability, but that does not always stay in the vicinity of the green surface. (a) Continuous time, original state space; (b) continuous time, augmented state space; (c) discrete time, augmented state space.

Using (R0), the modified dynamics of r is governed by

$$\frac{d}{dt}\epsilon = -\frac{1}{\tau_0}\epsilon, \tag{19}$$

$$\overset{(12)}{\Leftrightarrow} \frac{d}{dt}r = -\frac{1}{\tau_0} f_\epsilon(\mathbf{q}, r) + \frac{\partial_{\mathbf{q}} E_{nl}(\mathbf{q})^\intercal}{\sqrt{2E_{nl}(\mathbf{q}) + C_0}} \frac{d}{dt}\mathbf{q}, \tag{20}$$

$$\overset{(10a)}{\Leftrightarrow} \frac{d}{dt}r = -\frac{1}{\tau_0} f_\epsilon(\mathbf{q}, r) + \frac{\partial_{\mathbf{q}} E_{nl}(\mathbf{q})^\intercal \mathbf{M}^{-1}\mathbf{p}}{\sqrt{2E_{nl}(\mathbf{q}) + C_0}}, \tag{21}$$

which must replace the third line of the original system [Eqs. (13–15)]. To this end, the third line of matrix $\mathbf{J}_{\text{sav}}$ in Eq. (15) is modified, by considering (instead of $\mathbf{g} = \mathbf{g}_{\text{std}}$)

$$\mathbf{g}(\boldsymbol{\alpha}_{\text{sav}}) := \mathbf{g}_{\text{std}}(\mathbf{q}) + \mathbf{g}_{\text{mod}}(\boldsymbol{\alpha}_{\text{sav}}), \tag{22}$$

$$\mathbf{g}_{\text{mod}}(\boldsymbol{\alpha}_{\text{sav}}) = -\frac{1}{\tau_0} f_\epsilon(\mathbf{q}, r) \frac{\text{sign}(\mathbf{M}^{-1}\mathbf{p})}{||\mathbf{M}^{-1}\mathbf{p}||_{L^1}}, \tag{23}$$

where $\mathbf{g}_{\text{mod}}$ and $\mathbf{g}_{\text{std}}$, respectively, produce the first and the second right-hand term in Eq. (21).

Then, requirement (R1) is simply achieved by considering Eq. (22) also in the first line $\mathbf{J}_{\text{sav}}$ in Eq. (15) to preserve its skew symmetry. Finally, requirement (R2) is naturally fulfilled because $\mathbf{g}(\boldsymbol{\alpha}_{\text{sav}})$ is a first-order perturbation of $\mathbf{g}_{\text{std}}(\mathbf{q})$ with parameter $\epsilon = f_\epsilon(\mathbf{q}, r)$ and as $\frac{d}{dt}\epsilon = 0$ if $\epsilon = 0$.

To fulfill requirement (R1), note that the dynamics of $\mathbf{p}$ for the modified system have, however, been altered in cases where $\epsilon \neq 0$. To summarize, the method consists of adding $\mathbf{g}_{\text{mod}}$ to the standard $\mathbf{g}_{\text{std}}$ term in Eq. (15) and modifying the time-stepping scheme accordingly (see SEC. 5). Note that in Eq. (23), $\mathbf{g}_{\text{mod}}$ is singular at $\mathbf{p} = \mathbf{0}$. This issue is addressed in the numerical scheme by adding a small regularization parameter to the denominator of $\mathbf{g}_{\text{mod}}$.

5 ENERGY-PRESERVING NUMERICAL SCHEME

An efficient energy-preserving time-interleaved scheme for Eqs. (13–15) is built using a Störmer-Verlet scheme for the linear part of the wave equation coupled to a midpoint scheme for the SAV part [14]. For improved efficiency, it is helpful to treat some dissipative terms implicitly and others explicitly. In the following, the dissipation matrix is decomposed as $\mathbf{R} = \mathbf{R}_{\text{sv}} + \mathbf{R}_{\text{mid}}$ with $\mathbf{R}_{\text{mid}}$ diagonal and positive semidefinite and $\boldsymbol{R}_{\text{sv}}$ positive semidefinite. State variables are approximated by time series defined on interleaved grids as $\mathbf{p}^n$, $\mathbf{q}^{n+\frac{1}{2}}$, and r^n. These time series approximate the values of the continuous time functions at times $t^n = n\,dt$ and $t^{n+\frac{1}{2}} = (n+\frac{1}{2})dt$, where $dt = 1/f_{\text{s}}$ is the sample period. The forward difference operator $\delta_{t+} w^n = (w^{n+1} - w^n)/dt$ and forward averaging operator $\mu_{t+} w^n = (w^{n+1} + w^n)/2$ are used to define the scheme as

$$\begin{aligned}\delta_{t+}\mathbf{p}^n = &-\mathbf{K}\mathbf{q}^{n+\frac{1}{2}} - \mathbf{R}_{\text{sv}}\mathbf{M}^{-1}\mathbf{p}^n \\ &-\mathbf{R}_{\text{mid}}\mathbf{M}^{-1}\mu_{t+}\mathbf{p}^n - \bar{\mathbf{g}}^n \mu_{t+} r^n + \mathbf{G}_p \mathbf{u}^{n+1/2},\end{aligned} \tag{24}$$

$$\delta_{t+}\mathbf{q}^{n-\frac{1}{2}} = \mathbf{M}^{-1}\mathbf{p}^n, \tag{25}$$

$$\delta_{t+} r^n = (\bar{\mathbf{g}}^n)^\intercal \mathbf{M}^{-1}\mu_{t+}\mathbf{p}^n, \tag{26}$$

where $\bar{\mathbf{g}}^n$ is a consistent explicit evaluation of $\mathbf{g}$ at time step n. In this work, expressions given in Table 2 are used.

Table 2. Evaluation of $\bar{\mathbf{g}}^n$ without and with drift control.

Standard SAV	SAV with drift control
$\bar{\mathbf{g}}^n = \mathbf{g}_{\text{std}}(\mathbf{q}^{n+1/2})$	$\bar{\mathbf{g}}^n = \mathbf{g}_{\text{std}}(\mathbf{q}^{n+1/2}) + \mathbf{g}_{\text{mod}}(\mathbf{p}^n, \mu_{t+}\mathbf{q}^{n-1/2}, r^n)$

Independently of this choice, the scheme satisfies the discrete power balance

$$\begin{aligned}\frac{E^{n+1} - E^n}{dt} = &-\underbrace{(\mathbf{M}^{-1}\mu_{t+}\mathbf{p}^n)^\intercal \mathbf{R}\mathbf{M}^{-1}\mu_{t+}\mathbf{p}^n}_{P_{diss}^{n+1/2} \geq 0} \\ &+ \underbrace{(\mathbf{M}^{-1}\mu_{t+}\mathbf{p}^n)^\intercal \mathbf{G}_p \mathbf{u}^{n+\frac{1}{2}}}_{P_{ext}^{n+1/2}}\end{aligned} \tag{27}$$

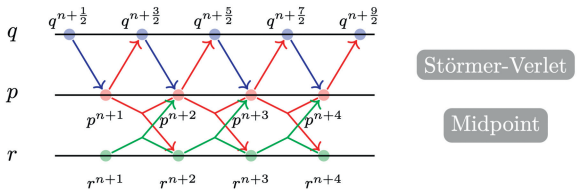


Fig. 2. Interpretation of the numerical scheme as the combination of a midpoint and a Störmer-Verlet scheme.

with pseudo-energy

$$E^n = \frac{1}{2}\left((\mathbf{p}^n)^\intercal \widetilde{\mathbf{M}}^{-1}\mathbf{p}^n + (\mu_{t+}\mathbf{q}^{n-\frac{1}{2}})^\intercal \mathbf{K}\mu_{t+}\mathbf{q}^{n-\frac{1}{2}} + (r^n)^2\right) \tag{28}$$

and modified mass matrix

$$\widetilde{\mathbf{M}}^{-1} = [\mathbb{I} - \frac{dt}{4}(dt\mathbf{M}^{-1}\mathbf{K}^\intercal + 2\mathbf{M}^{-1}\mathbf{R}_{\text{sv}})]\left(\mathbf{M}^{-1}\right). \tag{29}$$

The scheme is stable under the condition that the pseudoenergy is non-negative, which holds if $\widetilde{\mathbf{M}}^{-1}$ is positive definite. The stability condition thus depends only on a spectral analysis of the linear part of the system. Note that dissipative contributions evaluated with the midpoint effort estimate (corresponding to matrix $\mathbf{R}_{\text{mid}}$) are purely dissipative as $P_{diss}^{n+1/2} \geq 0$, whereas dissipative contributions evaluated explicitly (corresponding to matrix $\mathbf{R}_{\text{sv}}$) change the expression of the conserved pseudoenergy and the stability condition through modification of $\widetilde{\mathbf{M}}^{-1}$ in Eq. (29). This is the same as the case of backward difference approximations used in the case of linear string vibration [3].

Note that the standard SAV scheme can be interpreted as the combination of a Störmer-Verlet scheme between $\mathbf{q}$ and $\mathbf{p}$ with an interleaved midpoint scheme between $\mathbf{q}$ and r, as depicted in Fig. 2.

5.1 Update Form

Even though Eqs. (24–26) are semiexplicit, efficient update is in fact possible for systems having diagonal mass matrix $\mathbf{M}$. In [25], a first update form was presented, directly obtained from substitution of μ_{t+} and δ_{t+} operators in Eqs. (24–26). Here, instead, a further reduced version is presented. Using Eq. (25) to substitute the $\mathbf{p}^n$ and $\mathbf{p}^{n+1}$ vectors, one arrives at the following time-stepping algorithm on $\mathbf{q}$ only:

$$\bar{\mathbf{g}}^n = \mathbf{g}_{\text{std}}(\mathbf{q}^{n+1/2}) + \mathbf{g}_{\text{mod}}(\mathbf{p}^n, \mu_{t+}\mathbf{q}^{n-1/2}, r^n), \tag{30}$$

$$\mathbf{A}^n\mathbf{q}^{n+3/2} = \mathbf{B}\mathbf{q}^{n+1/2} + \mathbf{C}^n\mathbf{q}^{n-1/2} - \mathbf{g}^n r^n + \mathbf{G}_p\mathbf{u}^{n+1/2} \tag{31}$$

$$r^{n+1} = r^n + (\bar{\mathbf{g}}^n)^\intercal \frac{\mathbf{q}^{n+3/2} - \mathbf{q}^{n-1/2}}{2}, \tag{32}$$

with

$$\mathbf{A}^n = \left(\frac{\mathbf{M}}{dt^2} + \frac{\bar{\mathbf{g}}^n(\bar{\mathbf{g}}^n)^\intercal}{4} + \frac{\mathbf{R}_{\text{mid}}}{2dt}\right), \tag{33}$$

$$\mathbf{B} = \frac{2\mathbf{M}}{dt^2} - \mathbf{K} - \frac{\mathbf{R}_{\text{sv}}}{dt}, \text{ and} \tag{34}$$

$$\mathbf{C}^n = -\left(\frac{\mathbf{M}}{dt^2} - \frac{\bar{\mathbf{g}}^n(\bar{\mathbf{g}}^n)^\intercal}{4} - \frac{\mathbf{R}_{\text{mid}}}{2dt} - \frac{\mathbf{R}_{\text{sv}}}{dt}\right). \tag{35}$$

Leveraging the Sherman-Morrison inversion formula [15] to solve Eq. (31), one obtains

$$(\mathbf{A}^n)^{-1} = \mathbf{A}_0^{-1} - \frac{\mathbf{A}_0^{-1}\bar{\mathbf{g}}^n(\bar{\mathbf{g}}^n)^\intercal\mathbf{A}_0^{-1}}{4 + (\bar{\mathbf{g}}^n)^\intercal\mathbf{A}_0^{-1}\bar{\mathbf{g}}^n}, \tag{36}$$

$$\mathbf{A}_0^{-1} = 2dt^2[2\mathbf{M} + dt\mathbf{R}_{\text{mid}}]^{-1}, \tag{37}$$

where $\mathbf{M}$, $\mathbf{R}_{\text{mid}}$, and $\mathbf{A}_0$ are diagonal, allowing for efficient solving of Eq. (31).

5.2 Stability Condition for the String

The modified mass matrix for the discrete string model in Eqs. (7–10) reads

$$\widetilde{\mathbf{M}}^{-1} = \frac{1}{\rho A h}\left[\mathbb{I} + \left(\frac{dt^2}{4\rho A}(T\mathbb{I} - EI\mathbf{D}^2) + dt\eta_1\mathbb{I}\right)\mathbf{D}^2\right]. \tag{38}$$

The stability condition is directly obtained from noting that the lowest eigenvalue of $-\mathbf{D}^2$ is equal to $-\max(\lambda_{\mathbf{D}^2}) = -4/h^2$, and thus,

$$h \geq h_{\min} = \sqrt{\frac{\gamma + \sqrt{\gamma^2 + 16\rho AEIdt^2}}{2\rho A}}, \tag{39}$$

with $\gamma = dt^2T + 4dt\rho A\eta_1$.

5.3 Reference Scheme

In the following, a classical Störmer-Verlet scheme is used as a reference for comparison. Using the same notations and operators as before and $\delta_{tt}w^n = (w^{n+1} - 2w^n + w^{n-1})/dt^2$ and $\delta_{t\bullet}w^n = (w^{n+1} - w^{n-1})/2dt$, it may be written as

$$\delta_{tt}\mathbf{q}^n = \frac{1}{\rho A}\big[(T\mathbf{D}^2 - EI\mathbf{D}^4)\mathbf{q}^n - 2\rho A(\eta_0\mathbb{I} - \eta_1\mathbf{D}^2)\delta_{t\bullet}\mathbf{q}^n + \mathbf{f}_{nl}(\mathbf{q}^n) + \mathbf{G}_p\mathbf{u}^n\big] \tag{40}$$

and is easily adapted to the different forms of the nonlinearity. In the fully linear case, this scheme is subject to the same stability condition given by Eq. (39) and is fully explicit. However, in nonlinear cases, no stability condition is available, making it unsuitable for use directly in a real-time environment.

6 NUMERICAL EXPERIMENTS

This section presents results of numerical experiments performed on the string model using the proposed drift-controlled SAV method. First, the numerical power balance and convergence of the scheme are illustrated. Second, the effect of the new control term is studied and the choice of parameter τ_0 discussed.

During numerical testing, results for the GE and GE4 nonlinearities were found to be very nearly identical, equivalent in the range of amplitudes employed. For clarity of

Table 3. Fixed physical parameters.

$l_0 = 1.1$ m, $\rho = 8000$ kg.m^{-3}, $T = 60$ N, $E = 2 \times 10^{11}$ Pa
$\eta_0 = 0.9$ s^{-1}, $\eta_1 = 4 \times 10^{-4}$ m^{2}s^{-1}, $A = \pi(0.4 \times 10^{-3})^2$ m^2

the figures presented below, only the results corresponding to the GE4 nonlinearity are shown.

6.1 Power Balance and Convergence of the Scheme

Configuration: A string with fixed physical parameters given in Table 3 is used.

The external forcing term and initial velocity are set to zero. The initial displacement is set to correspond to the first modal shape of the linear string, or

$$\mathbf{q}^{-1/2} = \mathbf{q}^{1/2} = Q_0 \left[\sin\left(\frac{\pi}{N}\right), ..., \sin\left(\frac{(N-1)\pi}{N}\right) \right], \tag{41}$$

with amplitude Q_0. The auxiliary variable is initialized accordingly from the value of $\mathbf{q}^0 = \frac{1}{2}\left(\mathbf{q}^{-1/2} + \mathbf{q}^{1/2}\right)$. For a given sampling frequency, N is determined using the formula

$$N = 2 \left\lfloor \frac{\kappa\, l_0}{2h_{min}} \right\rfloor, \tag{42}$$

with $0 < \kappa \leq 1$ as a tuning parameter. Note that N is forced to be even because this ensures that the displacement at the middle of the string can be observed as $\hat{q} = \mathbf{q}_{N/2}$.

Power balance: A simulation with $Q_0 = 0.01$ m is run at $f_s = 44{,}100$ Hz and $h = h_{\min}$. The relative error on the energy balance, obtained as the error on Eq. (27) multiplied by dt/E^0 is on the order of machine precision in double-precision floating-point arithmetic, which shows that the scheme is indeed energy stable for quantities defined in the previous section. From Eq. (27), this result does not depend on the new control parameter τ_0, on the initial amplitude Q_0, or on the form of the nonlinear potential $E_{\text{nl}}(\mathbf{q})$.

Convergence: A set of $B = 6$ sampling frequencies $\{f_{s0}, 2f_{s0}, ..., 2^{B-1}f_{s0}\}$ Hz is used for simulations, with $f_{s0} = 44{,}100$ Hz. Reference solutions $\mathbf{q}_{ref}$ are built using the reference scheme from Eq. (40), with $f_s = 4 \times 2^{B-1} f_{s0}$ Hz. For each sampling frequency, N is computed using Eq. (42), with $\kappa = 0.9$.[4] Solutions are computed for a 0.1-s duration. The linear case and the three nonlinear cases presented in Table 1 are studied for different values of the initial amplitude Q_0. The relative L^2 error (decimated to sr_0) on the displacement of the middle of the string is used and computed as

$$\text{e}(\hat{\text{q}}, \hat{\text{q}}_{\text{ref}}) = \frac{||\hat{\text{q}} - \hat{\text{q}}_{\text{ref}}||^2}{||\hat{\text{q}}_{\text{ref}}||^2} \tag{43}$$

for each solution.

[4] In [25], the authors discussed the influence of κ on simulation results and showed that, in the nonlinear case, higher values of κ lead to a degradation of results, even though they result in a higher bandwidth, beneficial in the linear case.

Fig. 3 presents the convergence results for $\tau_0 = 0.001$ s. The results obtained with the original method from [14] are similar, indicating that the control term does not affect the formal rate of convergence and, therefore, are not reproduced here for clarity. In all configurations, the scheme converges asymptotically with a second-order slope with respect to the spatial discretization step h. For the linear and KC nonlinear cases (first row), errors are very small over the range of sampling frequencies and initial amplitudes employed here. The GE and GE4 nonlinearities are stronger, resulting in deteriorating performance with the initial amplitude because the system becomes numerically stiff. The yellow box highlights parameter ranges for which errors have not settled into a convergent pattern. Specifically, the scheme is expected to yield poor results for standard audio-rate $f_s = 44{,}100$ Hz and initial amplitudes greater than $Q_0 = 1$ cm.

Interestingly, reproducing Fig. 3 using the standard Störmer-Verlet scheme in Eq. (40) shows almost equivalent results, apart from the configurations corresponding to yellow boxes. In these configurations, the Störmer-Verlet scheme is unstable. The particular SAV scheme used in this paper (with or without the control method) is thus similar to Störmer-Verlet at lower amplitudes and serves to trade instability for imprecision at higher amplitudes. Although in a standard numerical analysis setting this trade-off would be of limited interest, in a real-time synthesis context, it is of great importance to the robustness of the algorithm.

6.2 Long-Term Behavior and Effect of the New Control Term

The effect of the control term is not visible on convergence curves. However, it greatly influences the long-term behavior of the simulations. Ideally, perceptual tests should be used to assess the effectiveness of the proposed method in real-world audio synthesis cases (i.e., with proper excitation signals). Because of the complexity of setting up such a test, the study here is limited to a qualitative study of the signal obtained from a repetitive struck-string configuration. Results are presented in Fig. 4. The string is set to have a fundamental frequency of $f_0 = 80$ Hz and is excited every second by a half-cosine force of duration 1 ms and maximum amplitude 5 N, as depicted in the top row. The second and third rows are obtained with the baseline SAV scheme. They depict, respectively, the evolution of the estimated fundamental frequency extracted from the output velocity at the middle of the string and of the absolute value of the drift abs (ϵ). The last two rows present the same results obtained with the proposed method and $\tau_0 = 0.001$ s.

The original explicit SAV algorithm from [14] leads to a severe drift of the SAV in the GE and GE4 cases. This is accompanied by a progressive drift of the fundamental frequency toward higher frequencies. Listening to the audio also reveals a strong degradation of the general signal quality, which quickly becomes polluted by noise. In contrast, results obtained using the proposed method show that the relative drift ϵ_{rel} [to the maximum observed value of

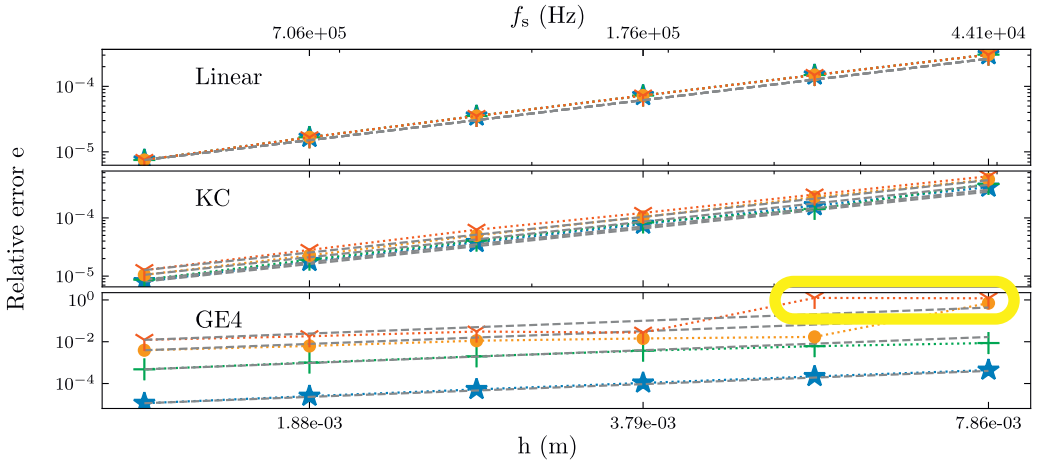


Fig. 3. Convergence study in the autonomous case, using relative error e as defined in Eq. (43) for the linear KC and GE4 models from Table 1 and for different values of the initial displacement amplitude Q_0. The control parameter is set to $\tau_0 = 0.001$ s. Gray dashed lines indicate second-order convergence slopes. The yellow boxes highlight points for which convergence has not started.

$E_{\text{nl}}(\mathbf{q})$ over the course of the simulation] stays low. Consequently, synthesis quality does not degrade after several strikes: pitch and harmonic content remain stable. Note that the pitch bends observed at each impact follow naturally from the nonlinearity of the model, which is excited at high amplitude.

Tuning the value of $\frac{1}{\tau_0}$ remains an open question. Indeed, it must ideally be as high as possible to be more responsive to a sudden increase in the value of ϵ, possible during high-amplitude transients. However, it is important to note that the numerical realization of the control law in Eq. (18) is not guaranteed to be convergent, even though the simulation itself is stable. The discrete time realization of Eq. (21) [see Eq. (26)] can be rewritten as

$$\delta_{t+} r^n - \mathbf{g}_{\text{std}}^{\intercal}(\mathbf{q}^{n+1/2})\mathbf{M}^{-1}\mu_{t+}\mathbf{p}^n = -\frac{1}{\tau_0}\epsilon(\mu_{t+}\mathbf{q}^{n-1/2}, r^n)\frac{\text{sign}(\mathbf{p}^n)^{\intercal}\mu_{t+}\mathbf{p}^n}{||\mathbf{p}^n||_{L^1}}. \quad (44)$$

The right hand term corresponds to the added control term and should ideally be equal to $-\frac{1}{\tau_0}\epsilon(\mathbf{q}^{n+1/2}, \mu_{t+}r^n)$ for the scheme to be centered (and thus second-order accurate). Instead, ϵ has to be evaluated at time step n to keep the scheme explicit. Worse, the multiplicative factor $\frac{\text{sign}(\mathbf{p}^n)^{\intercal}\mu_{t+}\mathbf{p}^n}{||\mathbf{p}^n||_{L^1}}$ is close to 1 for most of the oscillation cycle but can be locally negative if $\textbf{sign}(\mathbf{p}^n) \neq \textbf{sign}(\mu_{t+}\mathbf{p}^n)$. In this case, the control acts in a reverse sense. Note that the multiplicative factor has to be evaluated (and not simply replaced by 1) for the scheme to be energy stable. This problem, which limits the control effectiveness, remains unsolved.

6.3 Comparison With the Sign Constraint Method Developed in [22] and [21]

Because of the auxiliary variable drift, the original SAV algorithm has been shown to generate contact forces with reversed sign in the case of collision problems. In [22], the authors introduced a modification of the original algorithm to solve this issue, based on constraining the auxiliary variable to be positive. This guarantees that the effective nonlinear force as evaluated by the numerical scheme is of the

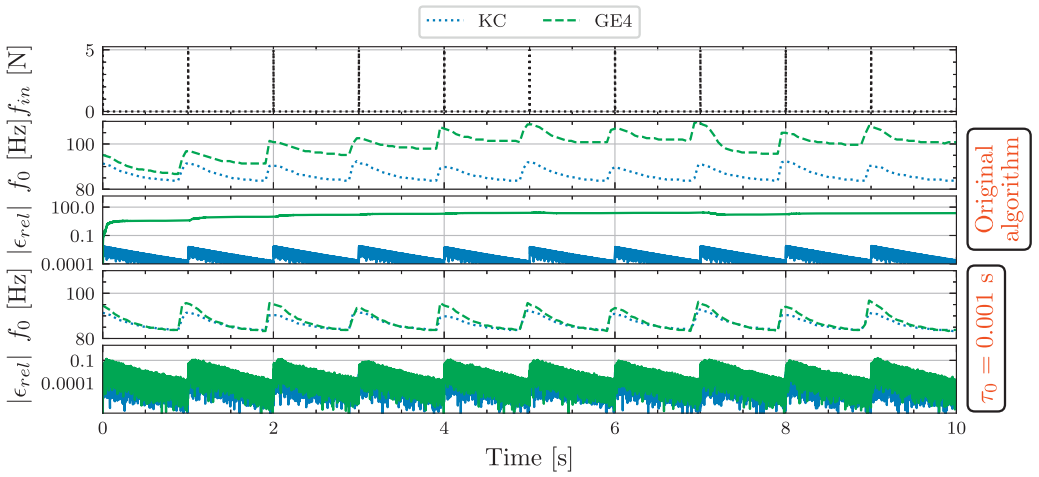


Fig. 4. Time series of fundamental frequency and auxiliary variable drift after successive hits on the string, without control (lines 2 and 3) and with the proposed method and $\tau_0 = 0.001$ s (lines 4 and 5).

correct sign, and greatly improves the results for collision problems.

For the string with GE or GE4 nonlinearity, Russo et al. [17] first identified the presence of an auxiliary variable drift, which is not present for the KC nonlinearity. In [21], the authors extend the constraint method proposed in [22] to the GE or GE4 nonlinearities and show a reduction of the auxiliary variable drift, associated with a better overall sound quality [or robust performance, as per requirement (C)].

However, the constraint approach suffers from a limitation for noncollision problems. Indeed, this constraint acts only if the auxiliary variable drifts toward negative values. The authors have observed that, depending on both the physical parameters of the model and the solver parameters (such as f_s and κ), the auxiliary variable can drift upward or downward (i.e., the solution can end up above or below the green surface in Fig. 1). If the auxiliary variable drifts upward, then the sign-constraint method is mostly ineffective. This motivates the development of the proposed method, which works independently of the direction of the drift.

From a control system viewpoint, the proposed method tries to solve the problem in a stronger sense than the sign-constraint method: instead of limiting the values of r to be positive, the proposed method aims at reducing the error between r and its reconstructed value from $\mathbf{q}$ through Eq. (11). In terms of reaction time, the sign-constraint method acts at a sample-accurate pace, whereas the proposed method needs some time to act (in the order of the characteristic control time τ_0). As an example, in the case of collisions, which generally happen over a few samples only, the proposed method is too slow to operate and the sign-constraint method is better suited.

It is interesting to note that the different methods can be combined by first computing $\mathbf{g}$ including the proposed control term, and then bounding it to apply the sign-constrain on the auxiliary variable, as done in [22] and [21]. The authors believe that the study of such a combination could be interesting in the future to handle, for example, strings with a geometric nonlinearity and a contact nonlinearity.

7 REAL-TIME IMPLEMENTATION

As a result of the explicit interleaved design, the algorithm presented here is efficient enough to run in a real-time audio environment. This section presents the implementation of the model as a Max/MSP external. It allows the instantiation of an object representing a single string with given physical parameters. Using multithreading, 60-note real-time polyphony was obtained. First, the framework used for this implementation is briefly presented, and then, the computational efficiency is examined.

7.1 Framework, Single String Implementation

The algorithm is implemented in C++ using the Eigen library for vector arithmetic. All matrix products are reduced to vector operations, noting that that difference matrices are at most pentadiagonal. The MinDevKit C++ API is used to define and build a Max/MSP object and is represented in Fig. 5. It presents the user with five audio-rate input signals and three audio-rate output signals.

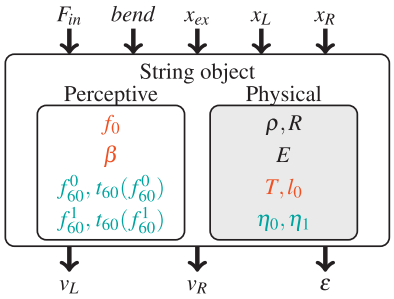


Fig. 5. Max/MSP object diagram.

The string model is excited locally by the scalar force signal F_{in} at position $x = \frac{x_{ex}}{l_0}$. $v_L := \partial_t u(x_L, t)$ and $v_R := \partial_t u(x_R, t)$ are velocity signals drawn from the string at two independent listening points ("pickups"), providing an artificial stereo audio output. First-order interpolation between two adjacent spatial grid points is performed, both for excitation and listening positions. A pitch bend signal is also provided to the object (see SEC. 7.3 for details on pitch bend implementation). The SAV variable drift ϵ is also generated as an output, mostly for monitoring and demonstration purposes and qualitative assessment of the effect of τ_0.

7.2 Physical Parameters

The physical constants of the string are not presented directly to the user. Instead, they are derived from a set of higher level perceptual parameters. ρ, R and E are fixed to a set of values corresponding to the string material. Given a fundamental frequency f_0 and inharmonicity factor β, T and l_0 are obtained as [5]

$$T = 2\pi f_0 \sqrt{\frac{EI\rho A}{\beta(1+\beta)}}, \quad l_0 = \frac{\pi}{2}\sqrt{\frac{EI}{\beta T}}. \tag{45}$$

The two dissipation coefficients η_0 and η_1 are computed from t_{60} decay times given at two frequencies, f_{60}^0 and f_{60}^1, using formulas given in [3, chapter 7].

7.3 Modulations

The first dissipation coefficient η_0 may be modulated in real-time without interfering with the stability condition because it does not intervene in Eq. (39). Modulation of this parameter allows the modification of bulk general damping by shifting the decay time curve vertically without changing its shape.

Real-time modulation of the other physical parameters is not straightforward because the stability condition depends on their values. In this work, small modulations of l_0 (and consequently h) are used to implement the pitch bend. An objective fundamental frequency is derived from the pitch bend signal (in cents) as $f_{bend} = f_0 \left(\frac{\text{bend}}{1200}\right)^2$. From this modified frequency and other physical parameters, a

[5] See [25] for more details.

Table 4. Real time ratios of the C++ Eigen implementation run on a MacBook Pro M3 for $f_s = 44{,}100$ Hz.

f_0 (Hz)	N	32 Bits (%)	64 Bits (%)	64-Bit original SAV (%)
20	360	3.6	7.3	5.3
50	215	2.2	4.1	3
100	140	1.5	2.7	2
200	84	0.99	1.6	1.2

Note. Different fundamental frequencies are used, resulting in different values of the spatial grid size N. Ratios are given for both 32-bit floating-point and 64-bit floating-point numbers. The last column presents the results for the original explicit SAV method from [14].

modified length l_{bend} is determined using Eq. (45). Finally, h is computed as

$$h = \max\left(\frac{l_{\text{bend}}}{N}, h_{\min}\right), \tag{46}$$

ensuring the stability of the simulation. Note that the maximum up-bend depends on the value of κ chosen at initialization.

7.4 Computational Efficiency and Polyphonic Synthesis

Table 4 presents the real-time ratios of the C++ implementation for different system sizes and floating-point number representations. Values are obtained as the ratio of the computing time and of the effective computed output duration. Simulations were run on a MacBook Pro M3 with $f_s = 44{,}100$ Hz for 20 s of effective output signal. Results for other sampling rates are not provided here for brevity but may be obtained simply by executing the timing script of the provided code. Compared with the original explicit SAV scheme from [14], the proposed method is near 40% more expensive, which is expected because the nonlinear function must be evaluated twice to obtain $\bar{g}^n$ in Eq. (33). However, the computational cost is still well below the real-time limit.

Indeed, for this hardware, 60-note polyphony can be obtained at $sr = 44{,}100$ Hz. This is done by duplicating the object presented in SEC. 7.1, and tuning each of the strings to a different note of the keyboard. The Max/MSP object poly$\sim$ is employed because it simplifies the duplication process in the Max/MSP environment, and more importantly, provides a direct access to multithreading. A load test patch reveals that the synthesis runs smoothly (without clicks resulting from buffer loss) for up to 60 strings, each with $N = 284$ spatial grid points, corresponding to a total of $\sim$20,000 degrees of freedom. This means that bigger systems resulting from discretization of 2D PDEs (e.g., plates or shells) could also potentially be run in real time. The current polyphonic patch allows for a great sonic diversity, given the unbounded range of possible decay times provided by the use of an energy-stable scheme and the possibility to tune the inharmonicity for bar-like sounds. The excitation signal corresponding to an input MIDI note is a half (for struck-like sound) or quarter (for pluck-like sound) sine of a given period, either given as an absolute value common to all strings or as a value relative to the fundamental period of the target string. The signal is scaled linearly with the MIDI velocity. Input and output gains can be tuned per string, allowing the nonlinearity to behave homogeneously across the keyboard. A dimensionless model would be more practical in this instance and will be implemented in the future.

8 CONCLUSION

In this study, a new numerical method is presented that extends the explicit time-interleaved SAV scheme presented in [14] to overcome the auxiliary variable drift problem—a key to achieving robust behavior suitable for musical use. It is based on the introduction of an additional control term in the continuous time equations only active in situations in which the auxiliary variable drifts.

Results of an application of this method to the simulation of a musical string with three types of nonlinearities are presented. As for the original SAV scheme, general convergence results remain to be proved. From a practical point of view, the results highlight a previously reported observation (see [17]) that, although in the Kirchhoff-Carrier case the drift does not appear, it greatly disturbs the results for the GE and GE4 nonlinearities. For these nonlinearities, the proposed modification enhances the long-term behavior of the simulation, preventing spurious pitch drifts and noise from building up as the string is struck multiple times. The computational efficiency remains relatively high, making the algorithm useful for real-time synthesis. The proposed Max/MSP implementation demonstrates a simple digital instrument based on the simulation of 60 uncoupled nonlinear strings excited by synthetic force signals. For more realism, one could model the exciter (i.e., hammer or bow) and couple strings together through a bridge. Note that these extensions may be formulated considering a passive coupling under a port-Hamiltonian representation such that the general methodology proposed in this paper would still be valid.

Future work includes more general numerical experiments on a broader category of dynamical systems. In the context of musical instrument modeling, collision problems are usually the most difficult to deal with and present the greatest challenge for the proposed method. First experiments show that the method is unfortunately too slow to react in the case of string collisions against frets. A hybrid between the proposed scheme and the collision-specific scheme developed in [22] seems like an interesting perspective for handling geometrical nonlinearities and collisions at the same time. Tests on 2D systems, such as nonlinear plate vibrations are also of interest, for e.g., drum or gong sound synthesis (see [19], where the explicit SAV method has been used for this purpose and where drift does pose a major problem). From a theoretical point of view, this paper presents one of many possible solutions for the stabilizing feedback law and the discrete evaluation of the proposed additional control term for which careful analysis may lead to refined choices.

9 ACKNOWLEDGMENT

This research was funded, in whole or in part, by l'Agence Nationale de la Recherche (ANR), Project AVATARS (ANR-22-CE48-0014).

10 REFERENCES

[1] J. O.III Smith, "Principles of Digital Waveguide Models of Musical Instruments," in M. Kahrs and K. Brandenburg (Eds.) *Applications of Digital Signal Processing to Audio and Acoustics*, The Int. Series in Engineering and Computer Science, vio. 437, pp. 417–466 (Springer, Boston, MA, 1998). https://doi.org/10.1007/0-306-47042-X_10.

[2] R. Caussé, J. Bensoam, and N. Ellis, "Modalys, A Physical Modeling Synthesizer: More Than Twenty Years of Researches, Developments, and Musical Uses," *J. Acoust. Soc. Am.*, vol. 130, no. 4_Supplement, p. 2365 (2011 Oct.). https://doi.org/10.1121/1.3654475.

[3] S. Bilbao, *Numerical Sound Synthesis: Finite Difference Schemes and Simulation in Musical Acoustics* (John Wiley & Sons, Chichester, UK, 2009). https://doi.org/10.1002/9780470749012.

[4] E. Hairer, C. Lubich, and G. Wanner, "*Structure-Preserving Algorithms for Ordinary Differential Equations: Geometric Numerical Integration*, Springer Series in Computational Mathematics, vol. 31 (Springer, Berlin, Germany, 2006), 2nd ed. https://doi.org/10.1007/3-540-30666-8.

[5] R. McLachlan, G. R. W. Quispel, and N. Robidoux, "Geometric Integration Using Discrete Gradients," *Phil. Trans. A Math. Phys. Eng. Sci.*, vol. 357, no. 1754, pp. 1021–1045 (1999 Apr.). https://doi.org/10.1098/rsta.1999.0363.

[6] E. Eich-Soellner and C. Führer, "Implicit Ordinary Differential Equations" in L. Arkeryd, H. Engl, A. Fasano, P. Neittaanmaki, and H. Neunzert (Eds.) *Numerical Methods in Multibody Dynamics*, pp. 139–192 (Springer Fachmedien Wiesbaden, Wiesbaden, Germany, 1998). https://doi.org/10.1007/978-3-663-09828-7.

[7] N. Lopes, T. Hélie, and A. Falaize, "Explicit Second-Order Accurate Method for the Passive Guaranteed Simulation of Port-Hamiltonian Systems," *IFAC-PapersOnLine*, vol. 48, no. 13, pp. 223–228 (2015 Oct.). https://doi.org/10.1016/j.ifacol.2015.10.243.

[8] B. M. Maschke and A. J. van der Schaft, "Port-Controlled Hamiltonian Systems: Modelling Origins and System Theoretic Properties," in *Nonlinear Control Systems Design 1992*, pp. 359–365 (1993 Jan.). https://doi.org/10.1016/S1474-6670(17)52308-3.

[9] A. van Der Schaft, "Port-Hamiltonian Systems: An Introductory Survey," in Proc. *Int. Cong. Mathematicians.*, pp. 1339–1365 (Madrid, Spain) (2006 Aug.). https://doi.org/10.4171/022-3/65.

[10] J. Zhao, Q. Wang, and X. Yang, "Numerical Approximations for a Phase Field Dendritic Crystal Growth Model Based on the Invariant Energy Quadratization Approach," *Int. J. Numer. Meth. Eng.*, vol. 110, no. 3, pp. 279–300 (2017). Apr.). https://doi.org/10.1002/nme.5372.

[11] J. Shen, J. Xu, and J. Yang, "The Scalar Auxiliary Variable (SAV) Approach for Gradient Flows," *J. Comput. Phys.*, vol. 353, pp. 407–416 (2018 Jan.). https://doi.org/10.1016/j.jcp.2017.10.021.

[12] S. Sato, "High-Order Linearly Implicit Exponential Integrators Conserving Quadratic Invariants With Application to Scalar Auxiliary Variable Approach," *Numer. Algorithms.*, vol. 96, no. 3, pp. 1295–1329 (2024 Jul.). https://doi.org/10.1007/s11075-024-01781-4.

[13] M. Ducceschi and S. Bilbao, "Simulation of the Geometrically Exact Nonlinear String via Energy Quadratisation," *J. Sound Vib.*, vol. 534, p. 117021 (2022 Sep.). https://doi.org/10.1016/j.jsv.2022.117021.

[14] S. Bilbao, M. Ducceschi, and F. Zama, "Explicit Exactly Energy-Conserving Methods for Hamiltonian Systems," *J. of Comput. Phys.*, vol. 472, p. 111697 (2023 Jan.). https://doi.org/10.1016/j.jcp.2022.111697.

[15] J. Sherman and W. J. Morrison, "Adjustment of an Inverse Matrix Corresponding to a Change in One Element of a Given Matrix," *Ann. Math. Stat.*, vol. 21, no. 1, pp. 124–127 (1950 Mar.). https://doi.org/10.1214/AOMS/1177729893.

[16] M. Ducceschi, M. Hamilton, and R. Russo, "Simulation of the Snare-Membrane Collision in Modal Form Using the Scalar Auxiliary Variable (SAV) Method," in Proc. *10th Conv. European Acoustic Association (Forum Acusticum)Forum Acusticum)*, pp. 1–7 (Torino, Italy) (2023 Sep.). https://doi.org/10.61782/fa.2023.0995.

[17] R. Russo, S. Bilbao, and M. Ducceschi, "Scalar Auxiliary Variable Techniques for Nonlinear Transverse String Vibration," *IFAC-PapersOnLine*, vol. 58, no. 6, pp. 160–165 (2024 Jun.). https://doi.org/10.1214/aoms/1177729893.

[18] M. van Walstijn, V. Chatziioannou, and N. Athanasopoulos, "An Explicit Scheme for Energy-Stable Simulation of Mass-Barrier Collisions With Contact Damping and Dry Friction," *IFAC-PapersOnLine*, vol. 58, no. 6, pp. 214–219 (2024 Jun.). https://doi.org/10.1016/j.ifacol.2024.08.283.

[19] S. Bilbao, C. Webb, Z. Wang, and M. Ducceschi, "Real-Time Gong Synthesis," in Proc. *26th Int. Conf. Digital Audio Effects*, pp. 1–8 (Copenhagen, Denmark) (2023 Sep.).

[20] G. Castera and J. Chabassier, "Numerical Analysis of Quadratized Schemes. Application to the Simulation of the Nonlinear Piano String," Technical Report 9516 (2023 Sep.). https://inria.hal.science/hal-04182465/.

[21] R. Russo, C. J. Webb, M. Ducceschi, and S. Bilbao, "Convergence Analysis and Relaxation Techniques for Modal Scalar Auxiliary Variable Methods Applied to Nonlinear Transverse String Vibration," In Proc. *Meetings on Acoustics*, vol. 56, no. 1, p. 035007 (New Orleans, LA) (2025 May). https://doi.org/10.1121/2.0002073.

[22] M. Van Walstijn, V. Chatziioannou, and A. Bhanuprakash, "Implicit and Explicit Schemes for Energy-Stable Simulation of String Vibrations With Collisions: Refinement, Analysis, and Comparison,"

J. Sound Vib., vol. 569, p. 117968 (2024 Jan.). https://doi.org/10.1016/j.jsv.2023.117968.

[23] M. Jiang, Z. Zhang, and J. Zhao, "Improving the Accuracy and Consistency of the Scalar Auxiliary Variable (SAV) Method With Relaxation," *J. Comput. Phys.*, vol. 456, p. 110954 (2022 May). https://doi.org/10.1016/j.jcp.2022.110954.

[24] Q.-A. Huang, C. Yuan, G. Zhang, and L. Zhang, "A Computationally Optimal Relaxed Scalar Auxiliary Variable Approach for Solving Gradient Flow Systems," *Comp. Math. Appl.*, vol. 156, pp. 64–73 (2024 Feb.). https://doi.org/10.1016/j.camwa.2023.12.017.

[25] T. Risse, T. Helie, and S. Bilbao, "Power-Balanced Drift Regulation for Scalar Auxiliary Variable Methods: Application to Real-Time Simulation of Nonlinear String Vibrations," in Proc. *28th Int. Conf. on Digital Audio Effects*, pp. 126–133 (Ancona, Italy) (2025 Sep.).

[26] P. Morse and U. Ingard, *Theoretical Acoustics* (Princeton University Press, Princeton, New Jersey, 1968).

[27] S. Bilbao, "Conservative Numerical Methods for Nonlinear Strings," *J. Acoust. Soc. Am.*, vol. 118, no. 5, pp. 3316–3327 (2005 Nov.). https://doi.org/10.1121/1.2046787.

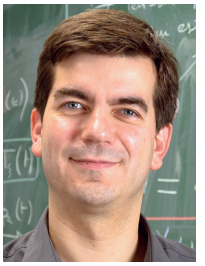
[28] V. Trenchant, H. Ramirez, Y. Le Gorrec, and P. Kotyczka, "Finite Differences on Staggered Grids Preserving the Port-Hamiltonian Structure With Application to an Acoustic Duct," *J. Comput. Phys.*, vol. 373, pp. 673–697 (2018 Nov.). https://doi.org/10.1016/j.jcp.2018.06.051.

[29] Q. Cheng, C. Liu, and J. Shen, "Generalized SAV Approaches for Gradient Systems," *J. Comput. Appl. Math.*, vol. 394, p. 113532 (2021 Oct.). https://doi.org/10.1016/j.cam.2021.113532.

THE AUTHORS


Thomas Risse


Stefan Bilbao


Thomas Hélie

Thomas Risse (Ph.D. in acoustics, Sorbonne Université, 2025) is currently a postdoctoral student at the Institute for Research and Coordination in Acoustics/Music (IRCAM). He is working on efficient methods for energy-balanced simulation of physical systems representing musical instruments and voice.

•

Stefan Bilbao (B.A. in physics, Harvard, 1992; M.Sc., Ph.D. in electrical engineering, Stanford, 1996 and 2001, respectively) is currently at the French National Centre for Scientific Research (CNRS Director of Research) based at the Institute for Research and Coordination in Acoustics/Music (IRCAM) in Paris. He has held previous positions at the University of Edinburgh and the Queen's University Belfast. He has been an associate editor of the *Institute of Electrical and Electronics Engineers (IEEE) Transactions on Audio Speech and Language Processing*, *Journal of the Acoustical Society of America* (*JASA*) *Express Letters*, and senior area editor for the *IEEE Open Journal of Signal Processing.*

•

Thomas Hélie [Ing. Dipl., Ecole nationale superieure (ENS) Telecommunications Bretagne, 1997; M.Sc., Ph.D. in control and signal processing, Univ. Paris-Saclay, 1998 and 2002, respectively; M.Sc. Acoustics, Signal Processing, and Informatics Applied to Music (ATIAM), Habilitation, Sorbonne Univ., 1998 and 2013, respectively] is Director of Research at the National Centre for Scientific Research (CNRS), head of the Sound Systems and Signals: Audio/Acoustics, instruMents (S3AM) team at the Sciences and Technologies of Music and Sound (STMS) Laboratory [Institute for Research and Coordination in Acoustics/Music (IRCAM)-CNRS-Sorbonne Univ.], and coordinator of the M.Sc. at ATIAM. His research spans nonlinear dynamical systems, control theory, signal processing, and acoustics applied to the physical modeling of musical/audio instruments and the voice. He has been a member of the French Acoustical Society (Musical Acoustics and Voice groups).